Advances in Applied Mathematics and Mechanics
Adv. Appl. Math. Mech., Vol. **1**, No. 4, pp. 546-572

DOI: 10.4208/aamm.09-m0924
August 2009

Hopf Bifurcations, Drops in the Lid–Driven Square Cavity Flow

Salvador Garcia*

Instituto de Matemáticas, Universidad Austral de Chile, Casilla 567, Valdivia, Chile

Received 16 March 2009; Accepted (in revised version) 14 April 2009
Available online 18 June 2009

Abstract. The lid-driven square cavity flow is investigated by numerical experiments. It is found that from Re= 5,000 to Re=7,307.75 the solution is stationary, but at Re=7,308 the solution is time periodic. So the critical Reynolds number for the first Hopf bifurcation localizes between Re=7,307.75 and Re=7,308. Time periodical behavior begins smoothly, imperceptibly at the bottom left corner at a tiny tertiary vortex; all other vortices stay still, and then it spreads to the three relevant corners of the square cavity so that all small vortices at all levels move periodically. The primary vortex stays still. At Re=13,393.5 the solution is time periodic; the long-term integration carried out past t_∞=126,562.5 and the fluctuations of the kinetic energy look periodic except slight defects. However at Re=13,393.75 the solution is not time periodic anymore: losing unambiguously, abruptly time periodicity, it becomes chaotic. So the critical Reynolds number for the second Hopf bifurcation localizes between Re=13,393.5 and Re=13,393.75. At high Reynolds numbers Re=20,000 until Re=30,000 the solution becomes chaotic. The long-term integration is carried out past the long time t_∞=150,000, expecting the time asymptotic regime of the flow has been reached. The distinctive feature of the flow is then the appearance of drops: tiny portions of fluid produced by splitting of a secondary vortex, becoming loose and then fading away or being absorbed by another secondary vortex promptly. At Re=30,000 another phenomenon arises—the abrupt appearance at the bottom left corner of a tiny secondary vortex, not produced by splitting of a secondary vortex.

AMS subject classifications: 76D05, 76F06

Key words: Navier-Stokes equations, Hopf bifurcations, chaos.

1 Introduction

The lid-driven square cavity flow has been investigated numerically. At low Reynolds numbers such as Re=100,1000,3,200, and 5,000, the solution is stationary; at mid

*Corresponding author.
Email: sgarcia@uach.cl (S. Garcia)

Reynolds numbers such as Re=7,500, 10,000, and 12,500, the solution is time periodic; at high Reynolds numbers such as Re=15,000, 17,500, and 20,000, the solution becomes chaotic. As the Reynolds number increases, three kind of solutions appear: stationary, time periodic, and chaotic. The results reported in [21] reveal that two Hopf bifurcations occur and that the critical Reynolds number for the first Hopf bifurcation localizes between Re=5,000 and Re=7,500 and the critical Reynolds number for the second Hopf bifurcation localizes between Re=12,500 and Re=15,000.

But yet, with precision, when and how changes the flow from stationary to time periodic and then from time periodic to chaotic?

This question which has not been addressed in [21] concerns in the first place this research, deserving much more attention because this is another source of disagreement when solving the lid-driven square cavity flow problem: in [25] the critical Reynolds number for the first Hopf bifurcation localizes between Re=7,500 and 10,000; in [14], approximate to Re=8,000; in [1], between Re=8,017.6 and 8,018.8; in [4,29,31], approximate to Re=7,402, Re=8,031.93, Re=8,000, respectively.

The present research determines two Hopf bifurcations with precision: within an interval of length 0.25 for the Reynolds number.

Indeed, from Re=5,000 to Re=7,307.75 the solution is stationary. But at Re=7,308 the solution is time periodic, not stationary. So the critical Reynolds number for the first Hopf bifurcation localizes between Re=7,307.75 and Re=7,308. Time periodical behavior begins smoothly, imperceptibly at the bottom left corner: at a tiny tertiary vortex—all other vortices stay still, and then it spreads to the three relevant corners of the square cavity—all small vortices at all levels move periodically. The primary vortex stays still. On the same hand, at Re=13,393.5 the solution is time periodic; the long-term integration carried out past t_∞=126,562.5, the fluctuations of the kinetic energy look periodic—except slight defects. But at Re=13,393.75 the solution is not time periodic anymore: losing unambiguously, abruptly time periodicity, it becomes chaotic. So the critical Reynolds number for the second Hopf bifurcation localizes between Re=13,393.5 and Re=13,393.75.

Yet, at high Reynolds numbers, for chaotic solutions, another question arises: when will they reach the time asymptotic regime of the flow, the global attractor [41, p. 104]—and how it looks like? In other words, once the numerical experiment runs for a sufficiently long time to make sure the time asymptotic regime of the flow has been reached, what are the distinctive features of the flow?

This interesting question partially addressed in [21] is the second concern of this research. In [21], it was partially addressed because the larger high Reynolds number considered was Re=20,000 and the long-term integration was carried out past the long time t_∞=25,000; whereas this research adds up three more high Reynolds numbers: Re=22,500, 25,000, 30,000, and the long-term integration is carried out past the long time $t_\infty \gg 25,000$.

Indeed, at high Reynolds numbers Re=20,000 until Re=30,000 the solution becomes chaotic. The long-term integration is carried out past the long time t_∞=150,000, expecting the time asymptotic regime of the flow has been reached. The distinctive

feature of the flow is then the appearance of drops: tiny portions of fluid produced by splitting of a secondary vortex, becoming loose and then fading away or being absorbed by another secondary vortex, promptly. At Re=30,000 another phenomenon arises—the abrupt appearance at the bottom left corner of a tiny secondary vortex, not produced by splitting of a secondary vortex.

Finally, one more question remains: what is the effect of the spatial mesh size refining on the computed solution?

This determinative question also partially addressed in [21] concerns in the third place of this research, partially addressed because the long-term integration was performed with h=1/128, 1/256 for stationary solutions and with h=1/256 for time periodic and chaotic solutions—h is the spatial mesh size; whereas to perform the long-term integration this research adds up two further refined mesh sizes h=1/512, 1/1024 when computing stationary solutions and one more further refined mesh size h=1/512 when computing time periodic solutions.

For stationary solutions, while not being reached yet, mesh convergence of numerical solutions seems to take place. It should appear for h equal to or smaller than h=1/2048, however. For time periodic solutions, a numerical experiment at a Reynolds number with h=1/256 seems to predict the one at a greater Reynolds number with h=1/512, making the former helpful for studying the time asymptotic regime of the flow.

The domain is the unit square cavity, and the viscous incompressible flow is governed by the two-dimensional time-dependent incompressible Navier-Stokes equations (NSE) [42] and driven by the upper wall, see Fig. 1. The nondimensionalized NSE in primitive variables with Dirichlet boundary conditions over the domain Ω= $[0,1]\times[0,1]$ read

$$\begin{cases} \dfrac{\partial \mathbf{u}}{\partial t} - \dfrac{1}{\mathrm{Re}}\Delta\mathbf{u} + (\mathbf{u}\cdot\nabla)\mathbf{u} + \nabla p = \mathbf{f}, & \text{in} \quad \Omega, \qquad t>0, \\ \nabla\cdot\mathbf{u} = 0, & \text{in} \quad \Omega, \\ \mathbf{u} = \boldsymbol{\varphi}, & \text{on} \quad \Gamma = \partial\Omega, \\ \mathbf{u}(\mathbf{x},0) = \mathbf{u}_0(\mathbf{x}), & \text{in} \quad \Omega, \end{cases} \tag{1.1}$$

where $\mathbf{u}$ is the velocity; p, the pressure; Re, the Reynolds number; $\mathbf{f}$, the external force. Here, $\mathbf{f}$=$\mathbf{0}$ and the boundary conditions read

$$\begin{cases} \mathbf{u}(\mathbf{x},\cdot) = (1,0), & \text{if } \mathbf{x} \in \text{upper wall}, \\ \mathbf{u}(\mathbf{x},\cdot) = \mathbf{0}, & \text{if } \mathbf{x} \in \text{left, bottom, or right wall}. \end{cases} \tag{1.2}$$

An unexpected balance of viscous and pressure forces makes the fluid to turn into the square cavity. The properties of these forces depending upon the Reynolds number, a hierarchy of vortices develops—the large clockwise-rotating primary vortex (1), whose location occurs toward the geometric center of the square cavity, and several small vortices: the counterclockwise-rotating secondary vortices (2), the clockwise-rotating tertiary vortices (3), the counterclockwise-rotating quaternary vortices (4), the

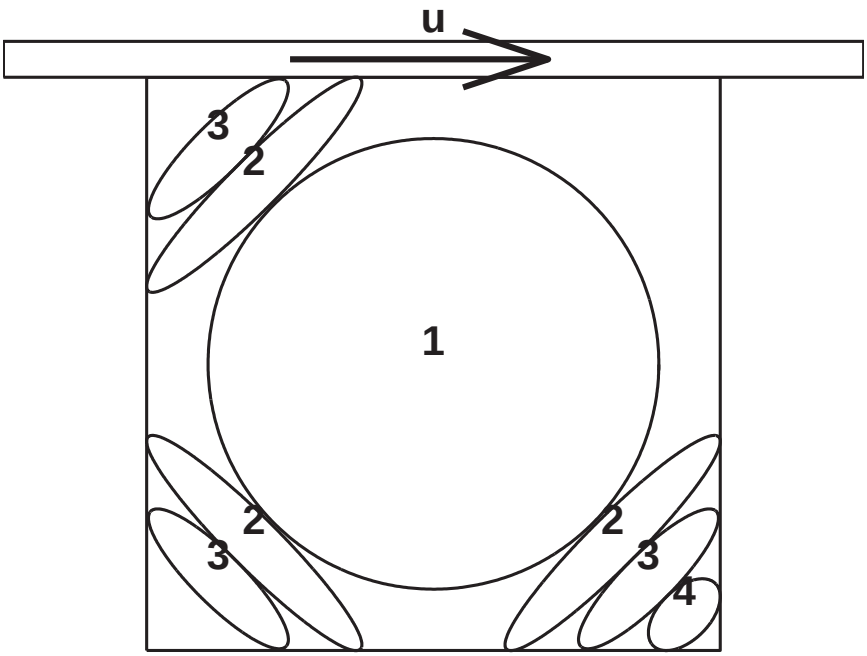

Figure 1: Flow past a square cavity.

clockwise-rotating quinary vortices (5), whose locations occur at the three relevant corners of the square cavity: bottom right (BR), bottom left (BL), and top left (TL), and appear hierarchically at the inclined ellipses as in Fig. 1.

Specifically, at the three relevant corners of the square cavity and at each level, secondary, tertiary, quaternary, and quinary one or two small vortices develop. If there is only one small vortex, this is named after the corresponding corner and the corresponding level, subscript; e.g., the bottom right tertiary vortex is named BR_3. If there are two small vortices, one occurs on the up side of the inclined ellipse; the other, on the down side. The corresponding prefix is added to the left of its name; e.g., the two bottom right secondary vortices are named upBR_2 and downBR_2.

A combination of known methods is used to discretize and solve the NSE: the linear Linθ^*-scheme [35] (a variant of the nonlinear θ-scheme [24]), the projection method [32], the Conjugate Gradient method [12], the Bi-CGSTAB method [43], the Fast Fourier Transform method [38, 39]—and the incremental unknowns method [5–11,15–22,25,30,36,37,40,45] as a spatial preconditioner. The linear Linθ^*-scheme is used for the temporal discretization—Δt is the time step—and a staggered marker-and-cell (MAC) mesh with finite-differences [26] is used for the spatial discretization—h is the spatial mesh size; see [21] for the theoretical as well as the graphics-presentation details.

This article is organized as follows. Section 2 displays the numerical experiments, ranging from Re=5,000 to Re=30,000; and Section 3 presents the conclusion.

2 Numerical experiments

Let us see what the numerical experiments reveal.

2.1 Stationary solutions

The case **Re**=**5,000**. The solution is stationary.

What is the effect of the spatial mesh size refining on the computed solution? Several spatial mesh sizes further and further refined are considered: h=1/128, 1/256, 1/512, 1/1024. And in each case the long-term integration is performed with the time step Δt=4h. Fig. 2 displays the complete phase diagram at the point $\mathbf{x}$=(7/8, 1/8): The 0 gray (black) line means the long-term integration is performed with the spatial mesh size h=1/1024, displayed first; the 0.25 gray line, h=1/512, sec-

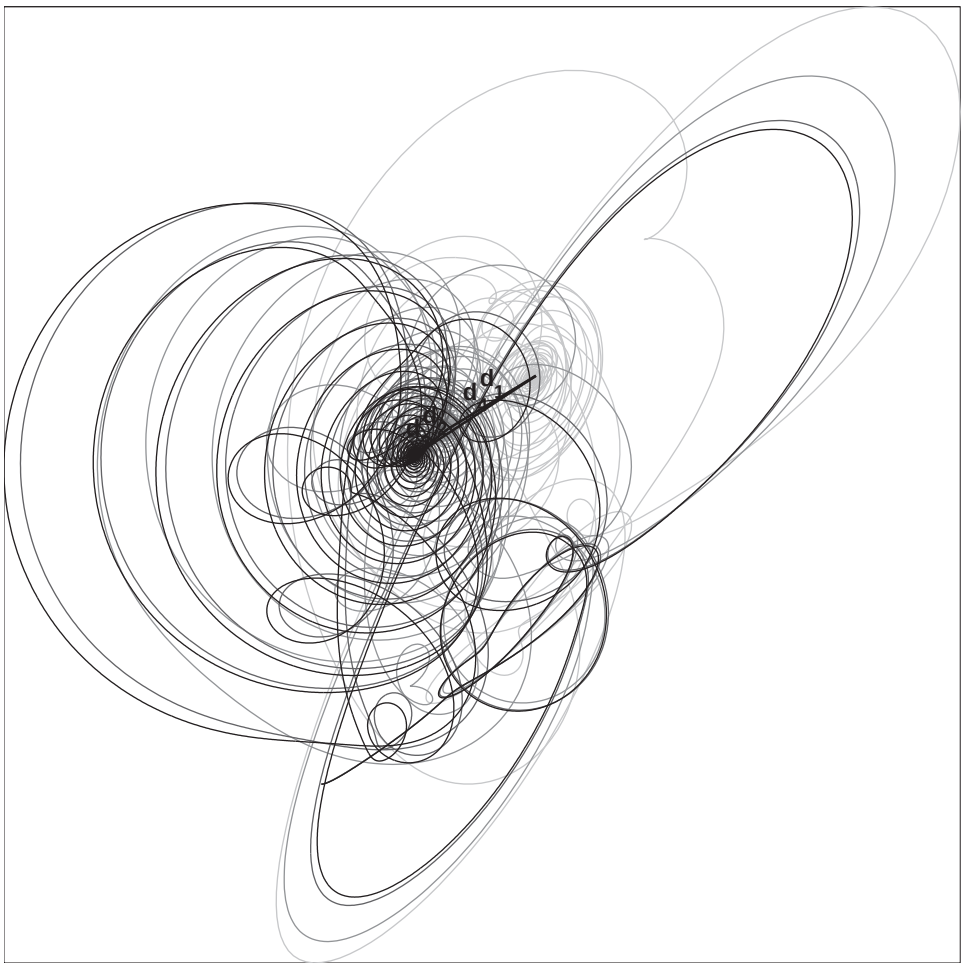

Figure 2: Re=5,000. The phase diagram at the point $\mathbf{x}$=(7/8, 1/8). Spatial mesh size refining.

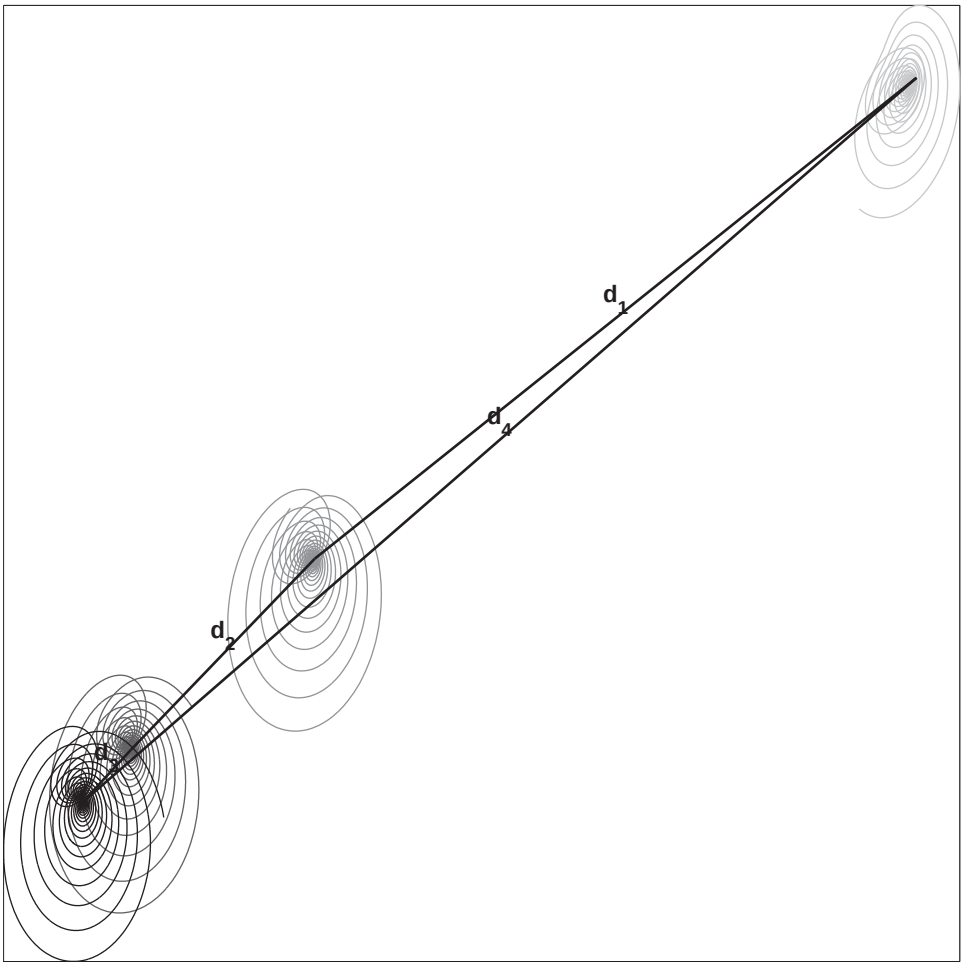

Figure 3: Re=5,000. The phase diagram at the point $\mathbf{x}=(7/8,1/8)$. Spatial mesh size refining. Detail.

ond; the 0.5 gray line, h=1/256, third; the 0.75 gray line, h=1/128, last. As the spatial mesh size is refined, the long-term behavior of the flow looks more and more similar to the previous one, and the distance between the end points of their plots significantly decreases, but the superposition of their plots is not reached yet: Fig. 3 displays the details. The distances are d_1=0.0072, d_2=0.0024, d_3=6.4790 $\times 10^{-4}$, d_4=0.0103. While not being reached yet, mesh convergence of numerical solutions seems to take place—It should appear for h equal to or smaller than h=1/2048, however.

2.2 The first Hopf bifurcation

At Re=7,307.75, the solution is stationary. But at Re=7,308 the solution is time periodic, not stationary. So the critical Reynolds number for the first Hopf bifurcation localizes between Re=7,307.75 and Re=7,308.

From the low Reynolds number Re=7,308 until the high Reynolds number Re=20,000—the primary vortex stays still.

2.3 Time periodic solutions

The case **Re=7,308**. The long-term integration is performed with $h=1/256, \Delta t=h$.

The solution is time periodic, not stationary. Fig. 4 displays this time periodic solution. For the most part, the solution's characteristics are as the ones of the case before Re=5,000 [21, p. 916]. But a distinctive feature adds up. Time periodical behavior begins smoothly, imperceptibly at the bottom left corner: at the tiny terciary vortex BL_3, which never dissapears; it is not noticeable elsewhere—all other small vortices stay still.

From now until otherwise stated, the long-term integration is performed with $h=1/256, \Delta t=4h$.

The case **Re=11,000**. The solution is time periodic.

Fig. 5 displays this time periodic solution. For the most part, the solution's behavior is as the one at the case before Re=10,000 [21, p. 922]. Yet, at the bottom right corner there is a secondary-secondary-quaternary vortex merging and splitting—and this is not sharp, cf. [21, page 923].

The case **Re=13,393.5**. The solution is still time periodic.

The long-term integration is carried out past t_∞=126,562.5. The fluctuations of the kinetic energy look periodic, except slight defects; Fig. 7 display the kinetic energy from t=126,484.390625 to t_∞=126,562.5. This long time reached, this time periodic behavior—except slight defects—do not seem to change abruptly, repeating on and on without noticeable changes.

The solution looks time periodic; Fig. 6 displays it, concentrating solely on the merging at the bottom right corner.

For the most part, the solution's behavior is as the one at the case before Re=12,500 [21, p. 923]—but at the bottom right corner.

At the bottom right corner, two secondary vortices downBR_2 and upBR_2 keep merging and splitting as time goes on. The merging and splitting are sharp. Immediately after the splitting, the tertiary vortex BR_3 becomes weak, and the primary vortex drags the secondary vortex upBR_2 downwards, to merge with the secondary vortex downBR_2—yet the merging is delayed. When the two secondary vortices downBR_2 and upBR_2 are going to merge, the quaternary vortex BR_4 arises and begins growing, spreading vertically upwards along the right wall, not merging with the secondary vortex upBR_2, and consequently not detaching the tertiary vortex BR_3 from the right wall. Afterwards, the quaternary vortex BR_4 spreads horizontally leftwards along the bottom wall. At this time, the tertiary vortex downBR_3 and the quaternary vortex upBR_4 form out. And then, the quaternary vortex downBR_4 and the tertiary vortex upBR_3 form out. The quaternary vortices downBR_4 and upBR_4 do not split; the quaternary vortex downBR_4 becomes sharp. Firstly, the interaction of the secondary vortex

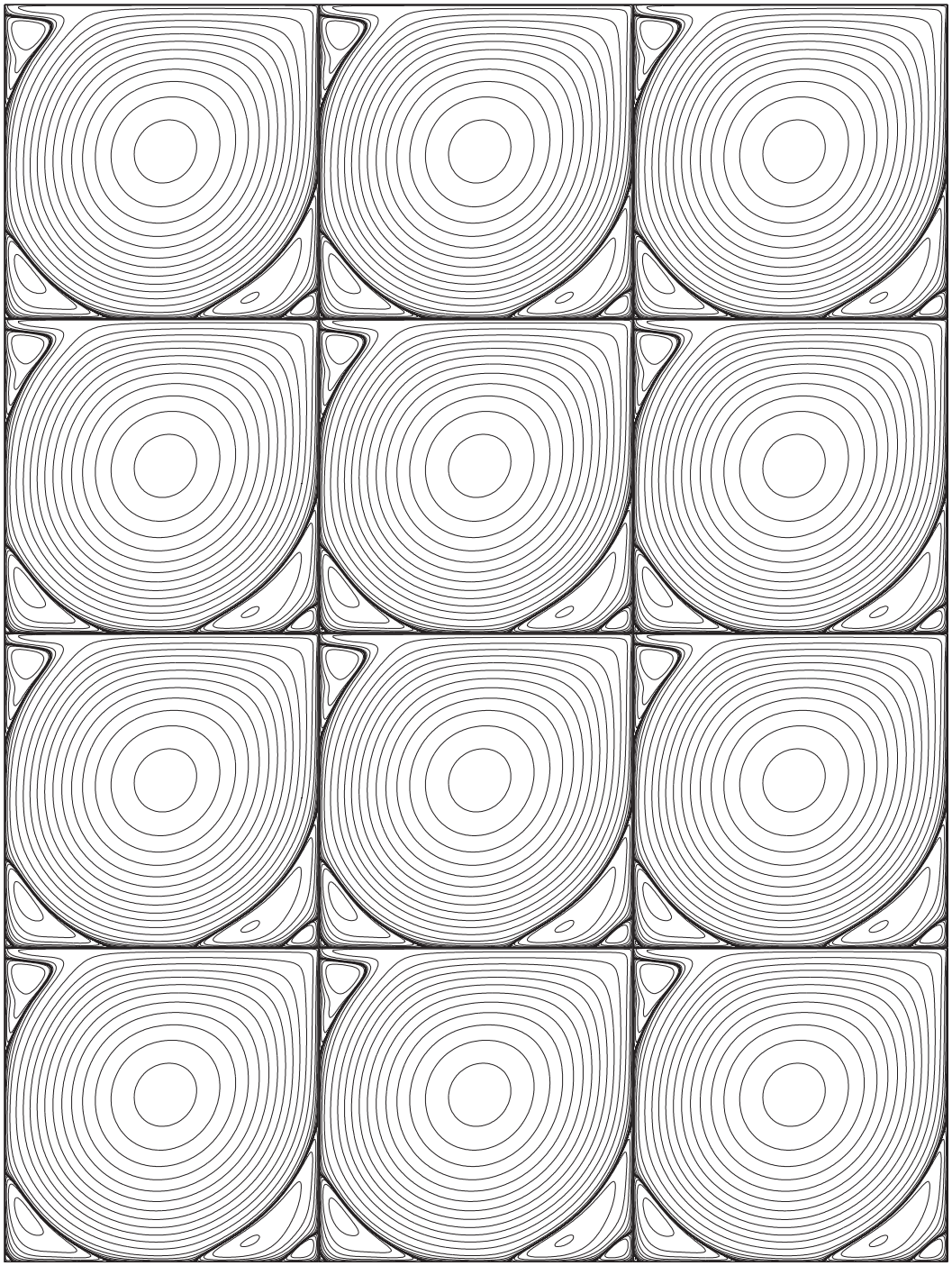

Figure 4: Re=7,308. h=1/256. Δt=h. Time periodic solution.

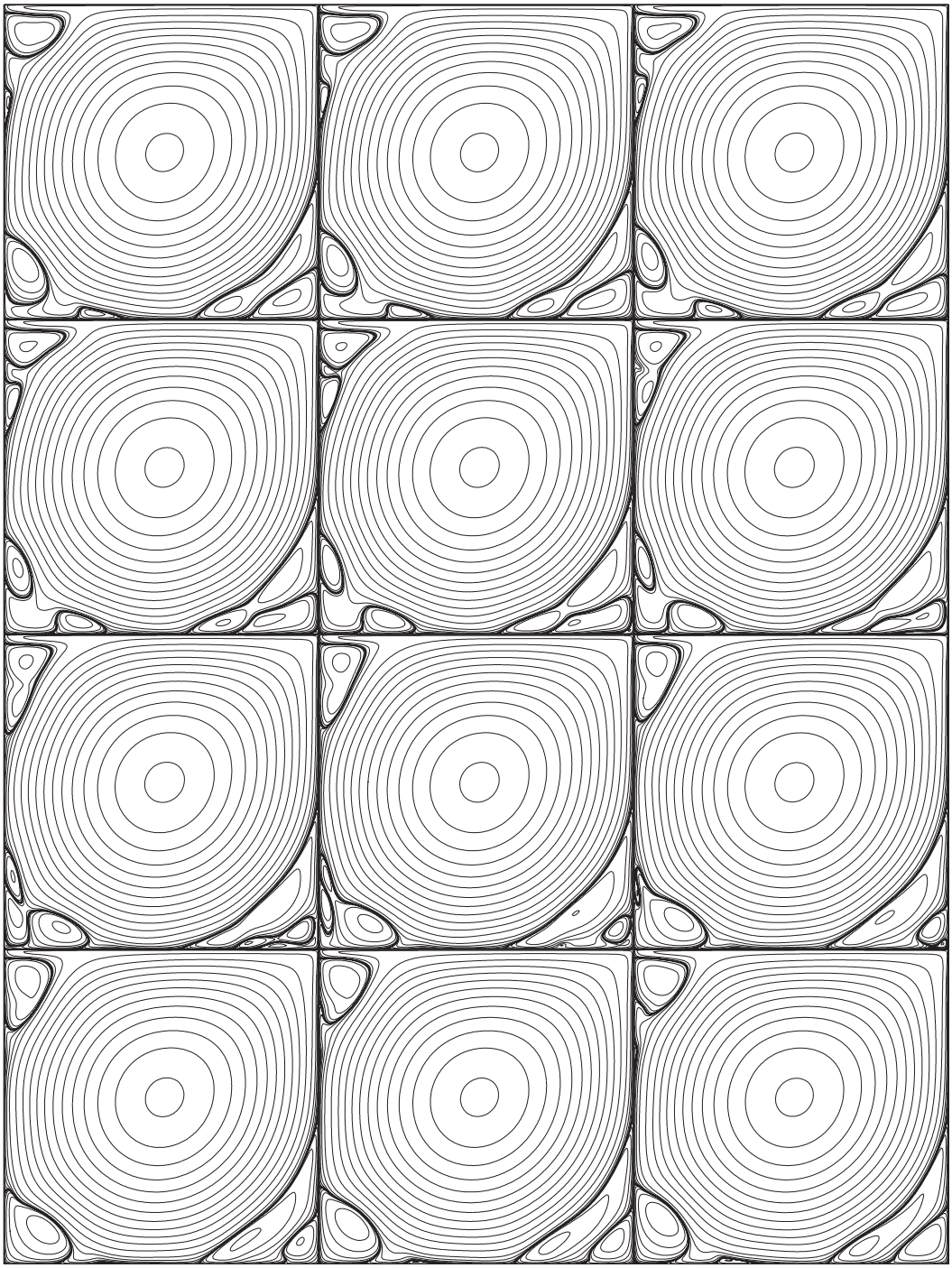

Figure 5: Re=11,000. h=1/256. Δt=4h. Time periodic solution.

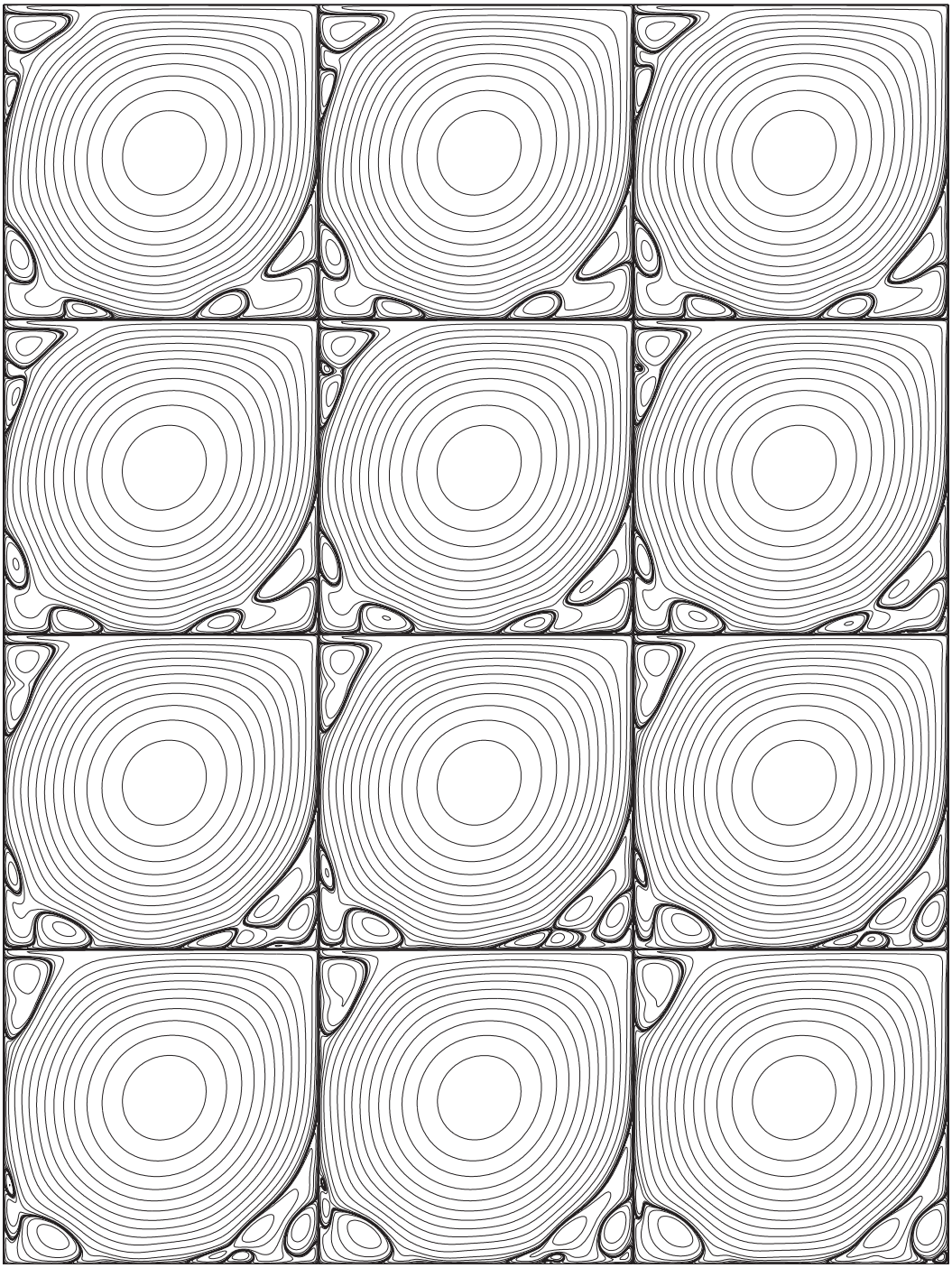

Figure 6: Re=13,393.5. h=1/256. Δt=4h. Time periodic solution.

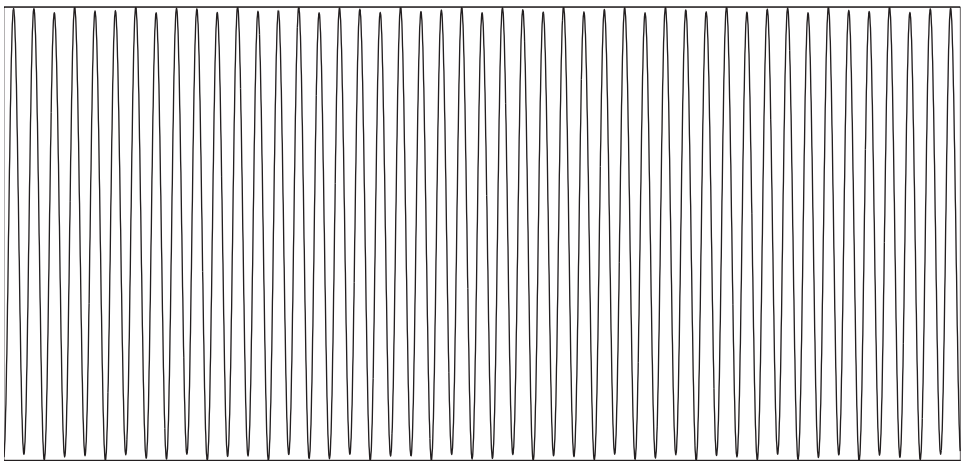

Figure 7: Re=13,393.5. h=1/256. Δt=4h. Kinetic energy.

upBR$_2$ and the quaternary vortex downBR$_4$ splits the tertiary vortex BR$_3$, giving rise to the tertiary vortices downBR$_3$ and upBR$_3$. Simultaneously, the secondary vortex upBR$_2$ and the quaternary vortex downBR$_4$ merge. Secondly, the secondary vortices upBR$_2$ and downBR$_2$ merge. Absorbing the secondary vortex downBR$_2$, destroying the tertiary vortex downBR$_3$, and dragged further downwards by the primary vortex, the secondary vortex upBR$_2$ becomes the secondary vortex BR$_2$. As the tertiary vortex downBR$_3$ vanishes, the quinary vortex BR$_5$ arises fleetingly. The tertiary vortex upBR$_3$ detached from the bottom wall but always clinging to the right wall becomes the tertiary vortex BR$_3$, the secondary vortex BR$_2$ dragging it upwards. And then, the quaternary vortex upBR$_4$ drags the tertiary vortex BR$_3$ downwards, making it to cling to the bottom wall. The tertiary vortex BR$_3$ splits the secondary vortex BR$_2$ and the quaternary vortex upBR$_4$, giving rise to the quaternary vortex BR$_4$. The tertiary vortex BR$_3$ and the quinary vortex BR$_5$ merge. And the quaternary vortex BR$_4$ detached from both the right wall and the bottom wall vanishes promptly. This is the secondary-quaternary-secondary vortex merging at the bottom right corner which followed by the splitting of the two secondary vortices downBR$_2$ and upBR$_2$ repeat, periodically, constituting the secondary-quaternary-secondary vortex merging and splitting at the bottom right corner.

2.4 The second Hopf bifurcation

At Re=13,393.5, the solution is time periodic. But at Re=13,393.75 the solution is not time periodic anymore: losing unambiguously, abruptly time periodicity, it becomes chaotic. So the critical Reynolds number for the second Hopf bifurcation localizes between Re=13,393.5 and Re=13,393.75.

2.5 Chaotic solutions

The case **Re**=**13**, **393**.**75**. The solution becomes chaotic.

The long-term integration is carried out past t_∞=54, 687.5. In the first place, the fluctuations of the kinetic energy look periodic—except slight defects; Fig. 8, top, display the kinetic energy from t=42, 187.5 to t=42, 265.609375. In the second place, the fluctuations of the kinetic energy change unambiguously, abruptly from periodic—except slight defects—to chaotic; Fig. 8, middle, display the kinetic energy from t=48, 593.75 to t=50, 624.953125. In the third place, the fluctuations of the kinetic energy definitely became chaotic; Fig. 8, bottom, display the kinetic energy from t=54, 609.390625 to t_∞ = 54, 687.5.

Let us see why at Re=13, 393.75 the solution becomes chaotic. And let us concentrate on the merging of secondary vortices, so let us consider the two secondary

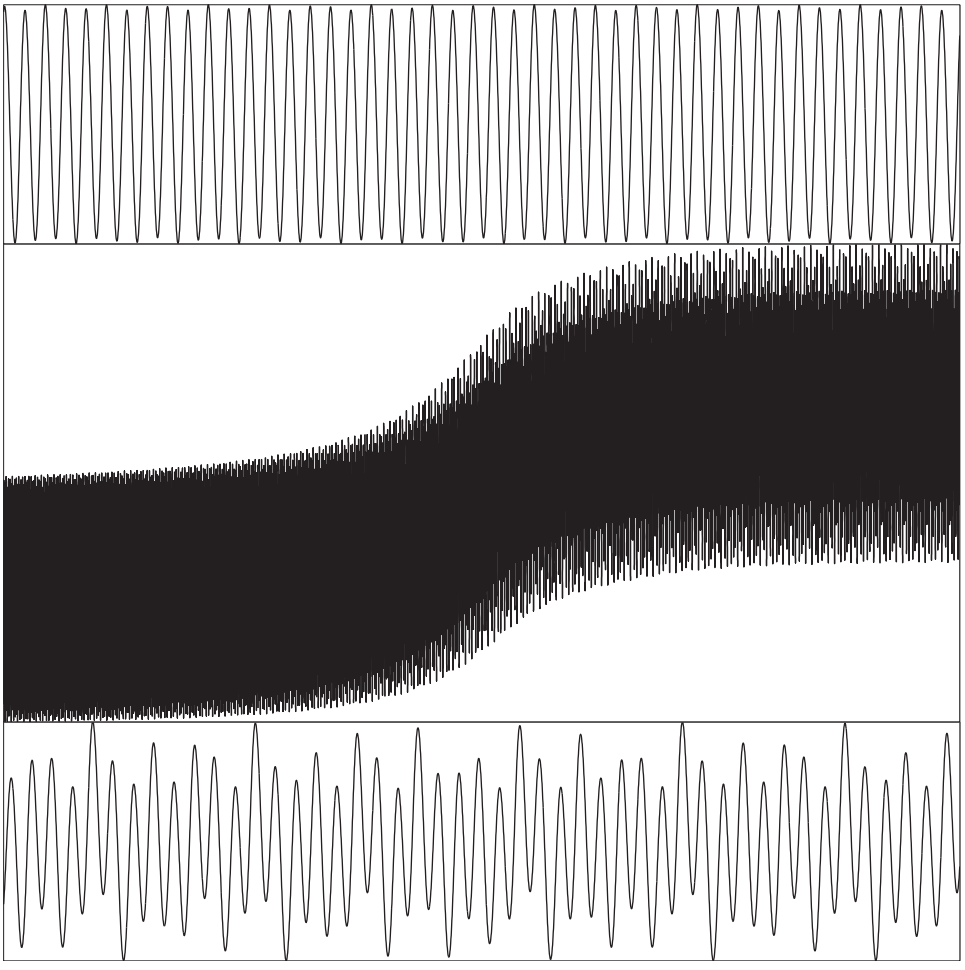

Figure 8: Re=13, 393.75. h=1/256. Δt=4h. Kinetic energy.

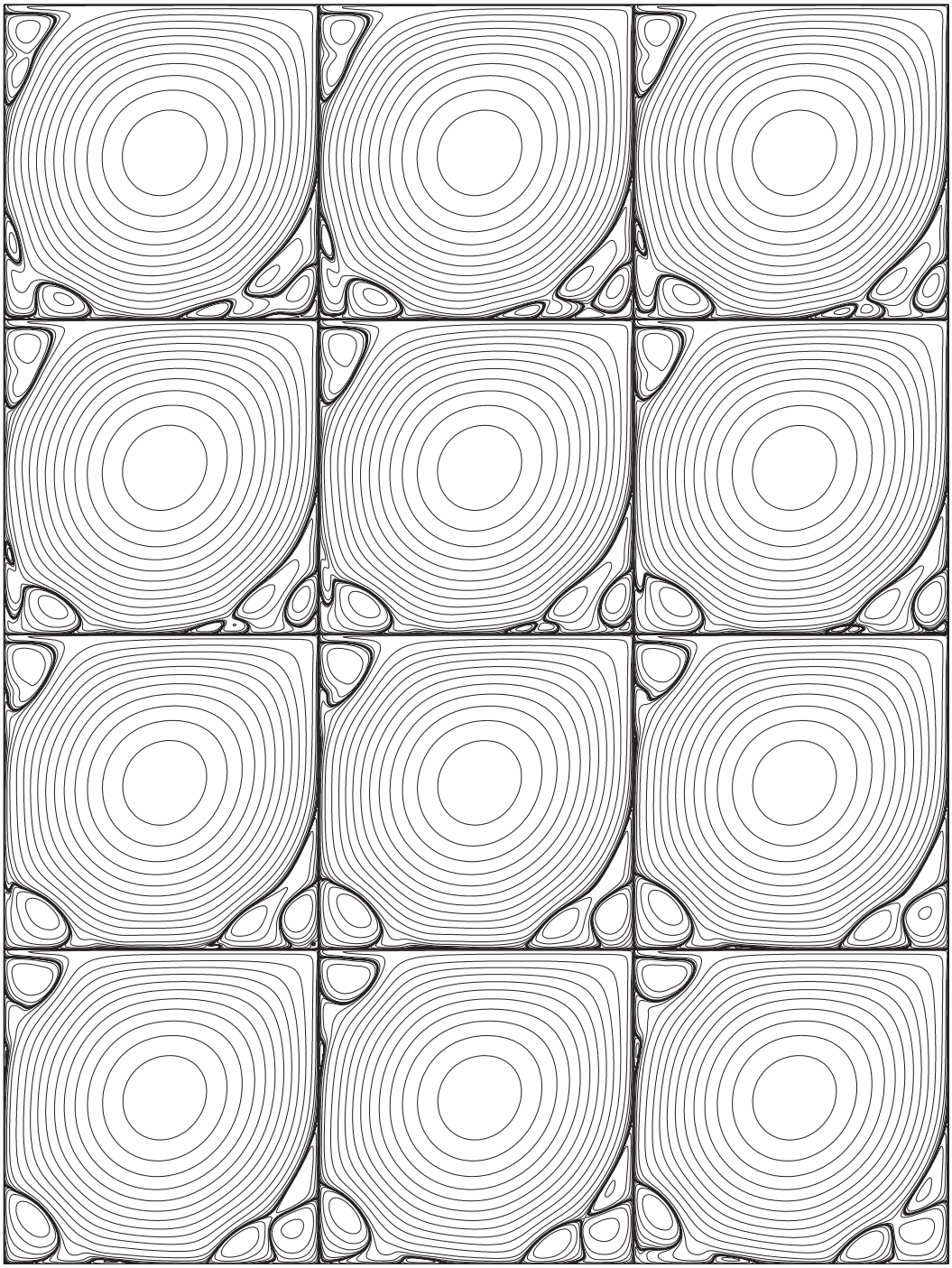

Figure 9: Re=13,393.75. h=1/256. Δt=4h. Chaotic solution. First occurrence.

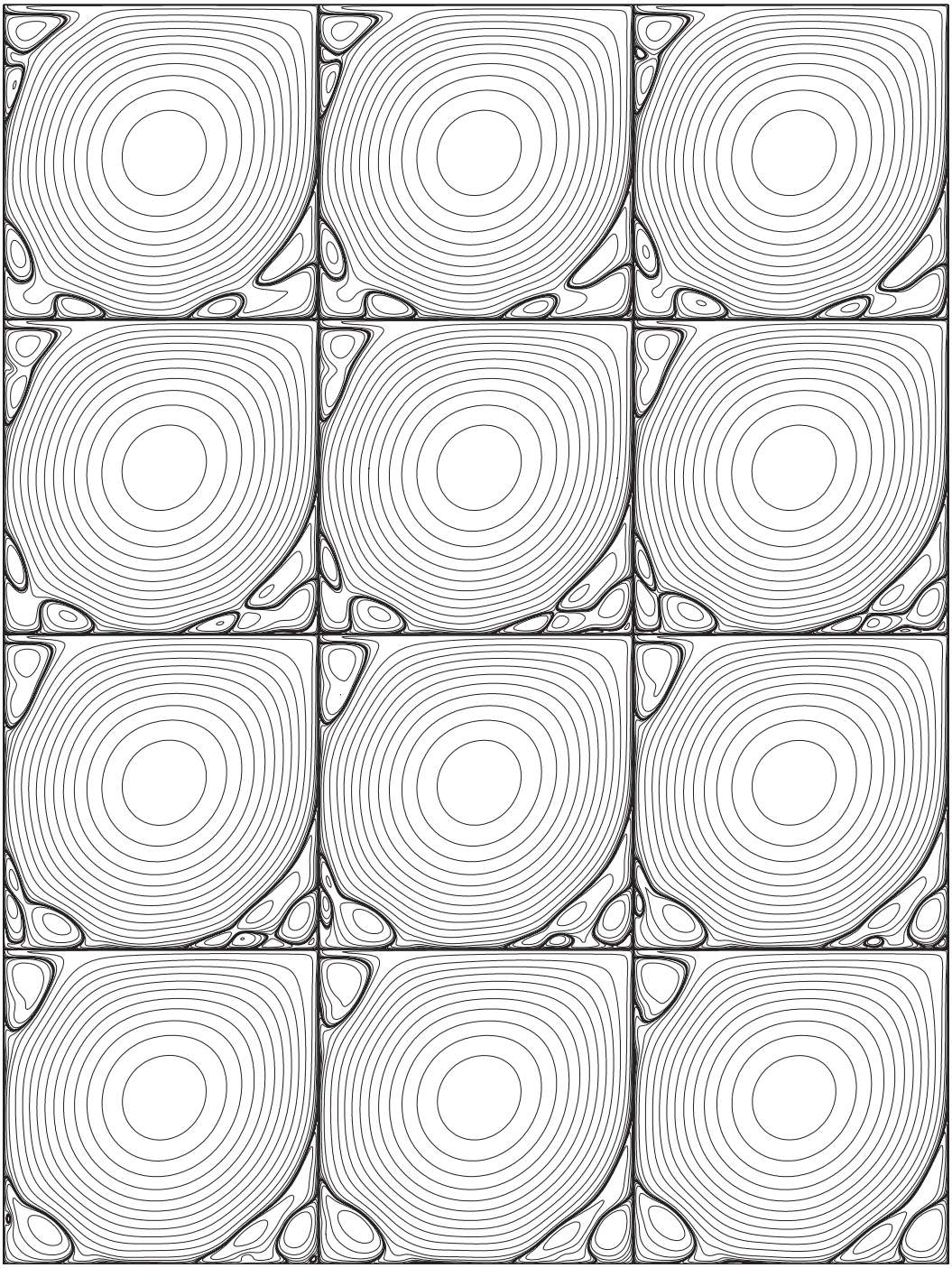

Figure 10: Re=13,393.75. h=1/256. Δt=4h. Chaotic solution. Second occurrence.

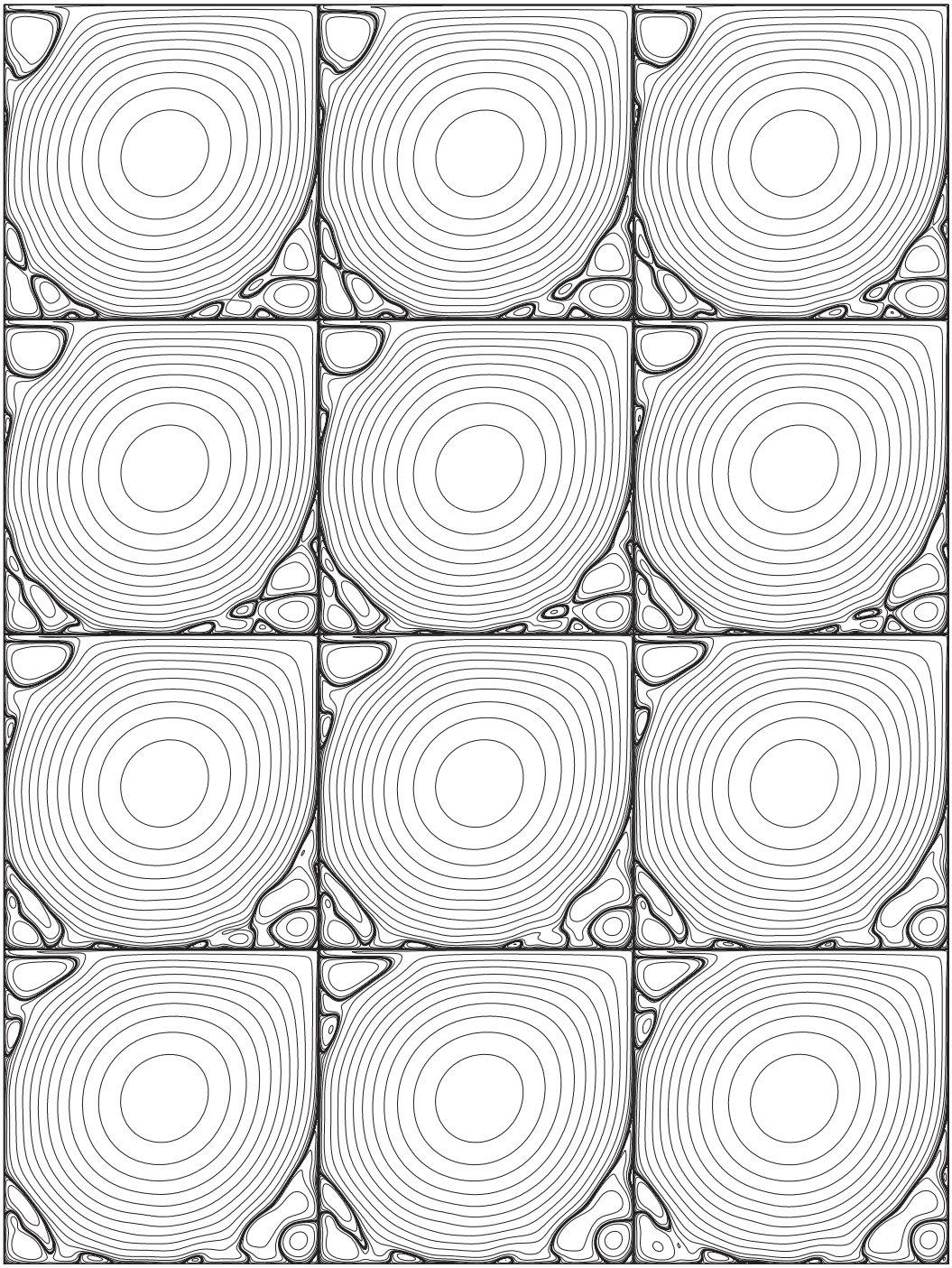

Figure 11: Re=20,000. h=1/256. Δt=4h. Chaotic solution. A particular occurrence.

vortices at the three relevant corners of the square cavity solely when they are going to merge—at two different occurrences.

Fig. 9 displays a first occurrence. At the bottom right corner, there is a distinct secondary-quaternary-secondary vortex merging. At the bottom left corner, there is a secondary-secondary vortex merging, but the merging do not occur: the secondary vortex upBL_2 disappears long before any merging with the secondary vortex downBL_2 can occur. At the top left corner, there is a secondary-secondary vortex merging.

Fig. 10 displays a second occurrence. At the bottom right corner, there is a distinct secondary-secondary-quaternary vortex merging. At the bottom left corner and at the top left corner, there is a secondary-secondary vortex merging.

Definitely, at Re=13,393.75 the solution is not time periodic anymore: losing unambiguously, abruptly time periodicity, it becomes chaotic. At the three relevant corners of the square cavity, the mergings, and the splittings if there are, repeat on and on, but not exactly the same as they do for time periodic solutions. The solution becomes chaotic because it loses time periodicity in these manners:

- The kind of merging may not be the same. At the bottom right corner, a merging follows a splitting which follows a merging and so on, but one merging may be a secondary-secondary-quaternary vortex merging, and another may be a secondary-quaternary-secondary vortex merging. At the bottom left corner, a merging follows a merging which follows a merging and so on, but sometimes the merging occurs and at other times do not.
- The size of the small vortices varies from occurrence to occurrence, not repeating exactly the same.

For the next high Reynolds numbers, the solution becomes chaotic, indeed. And the long-term integration is carried out past the long time t_∞=150,000, expecting the time asymtotic regime of the flow has been reached. Let us focus our attention on some phenomena appearing after this long time has been reached.

The case **Re=20,000**. The solution becomes chaotic.

Fig. 11 displays a particular occurrence. The distinctive feature is a drop. At the bottom right corner. Starting on entry $(1,3)$ and ending on entry $(3,1)$, the interaction of the primary vortex and the strong tertiary vortex upBR_3 pinches off a drop from the secondary vortex upBR_2, a drop which is dragged downwards by the primary vortex to merge with the secondary vortex downBR_2 but which vanishes just before the merging can occur.

From now on, the primary vortex do not stay still anymore.

The case **Re=22,500**. The solution becomes chaotic.

Fig. 12 displays a particular occurrence. The distinctive feature is a drop. At the bottom left corner. Starting on entry $(2,1)$ and ending on entry $(4,3)$, the shape of the secondary vortex downBL_2 contributing, the strong action of the primary vortex detaches a drop from the secondary vortex downBL_2. The primary vortex drags the

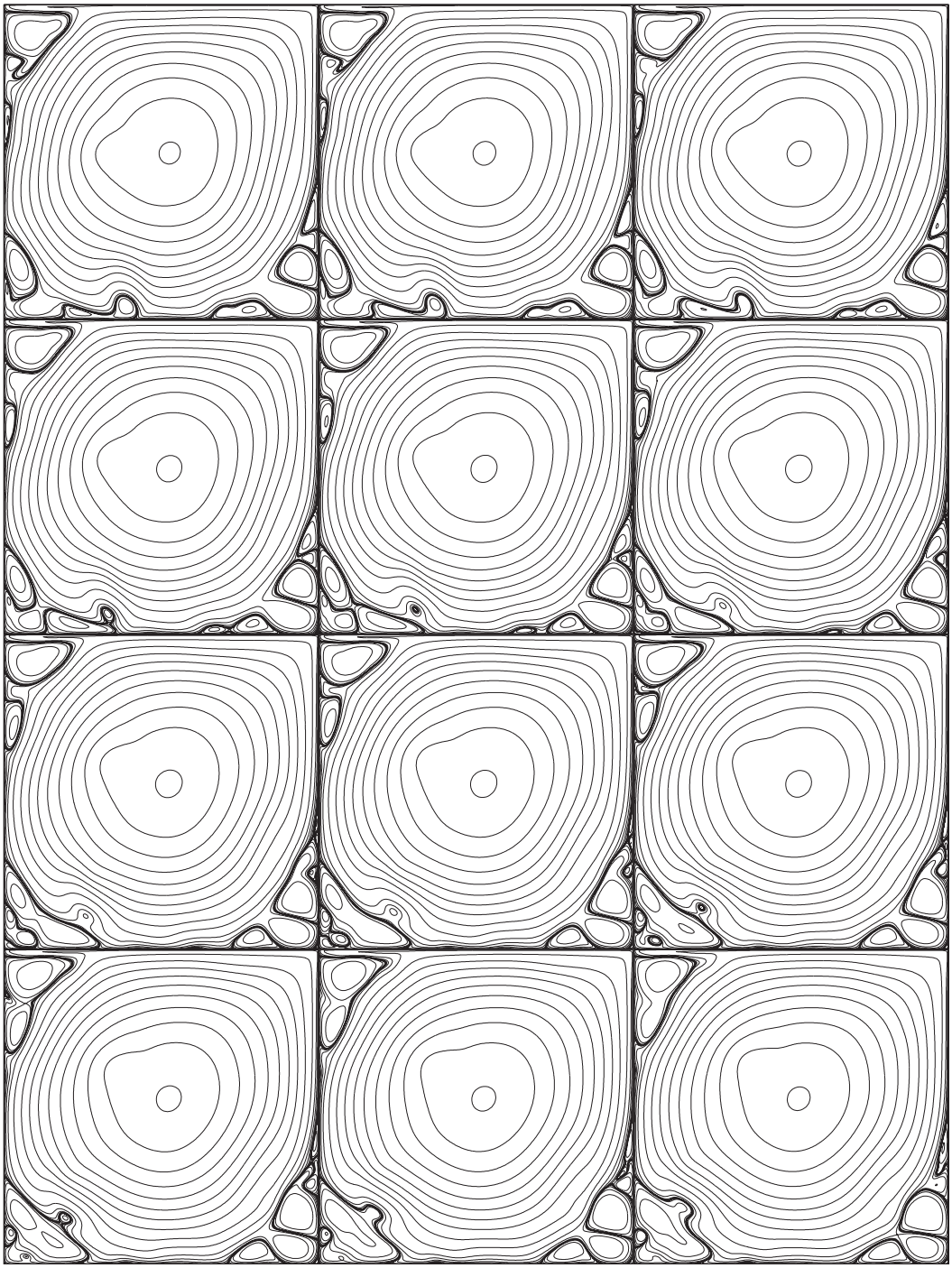

Figure 12: Re=22,500. h=1/256. Δt=4h. Chaotic solution. A particular occurrence.

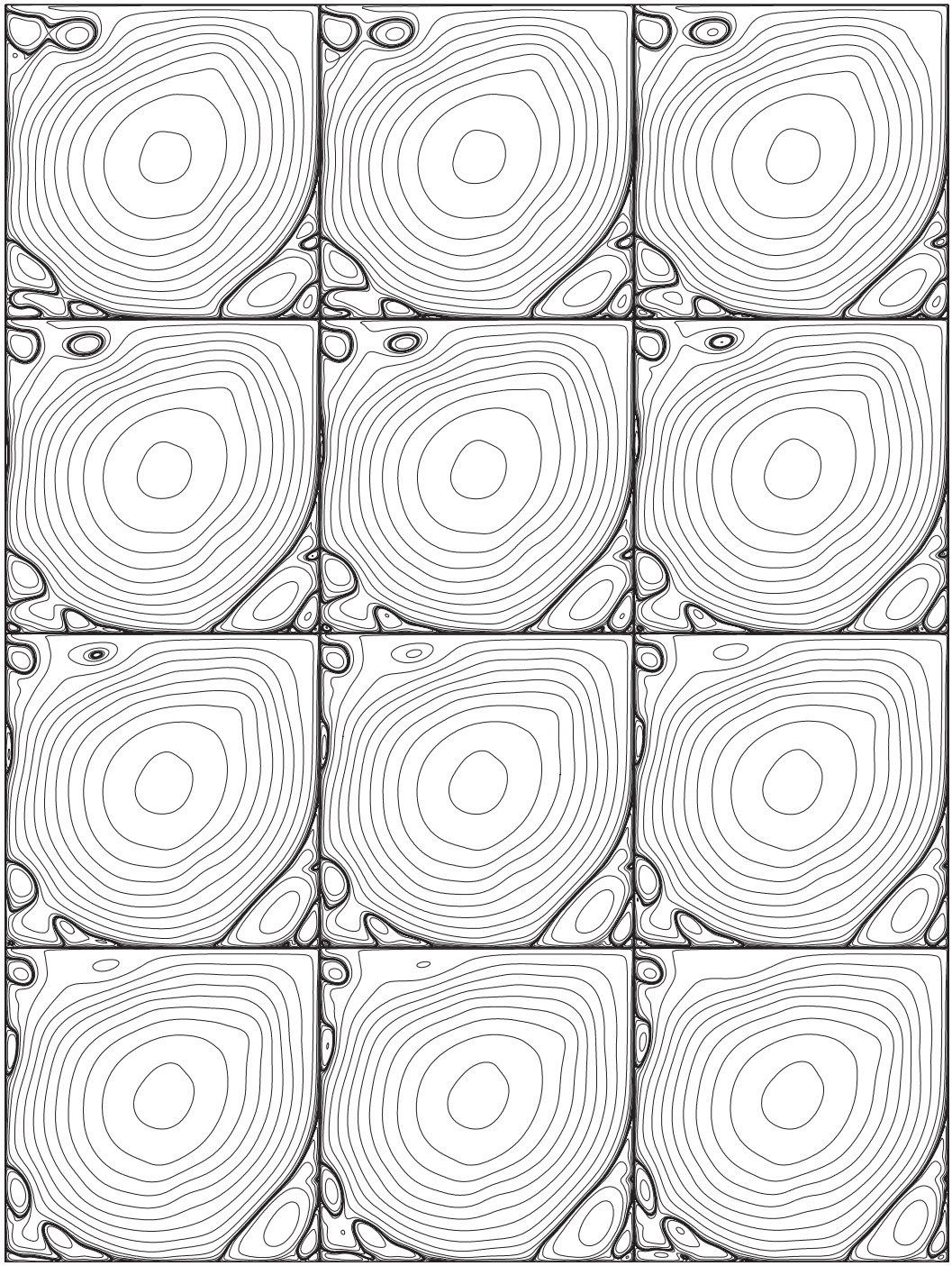

Figure 13: Re=25,000. h=1/256. Δt=4h. Chaotic solution. A particular occurrence.

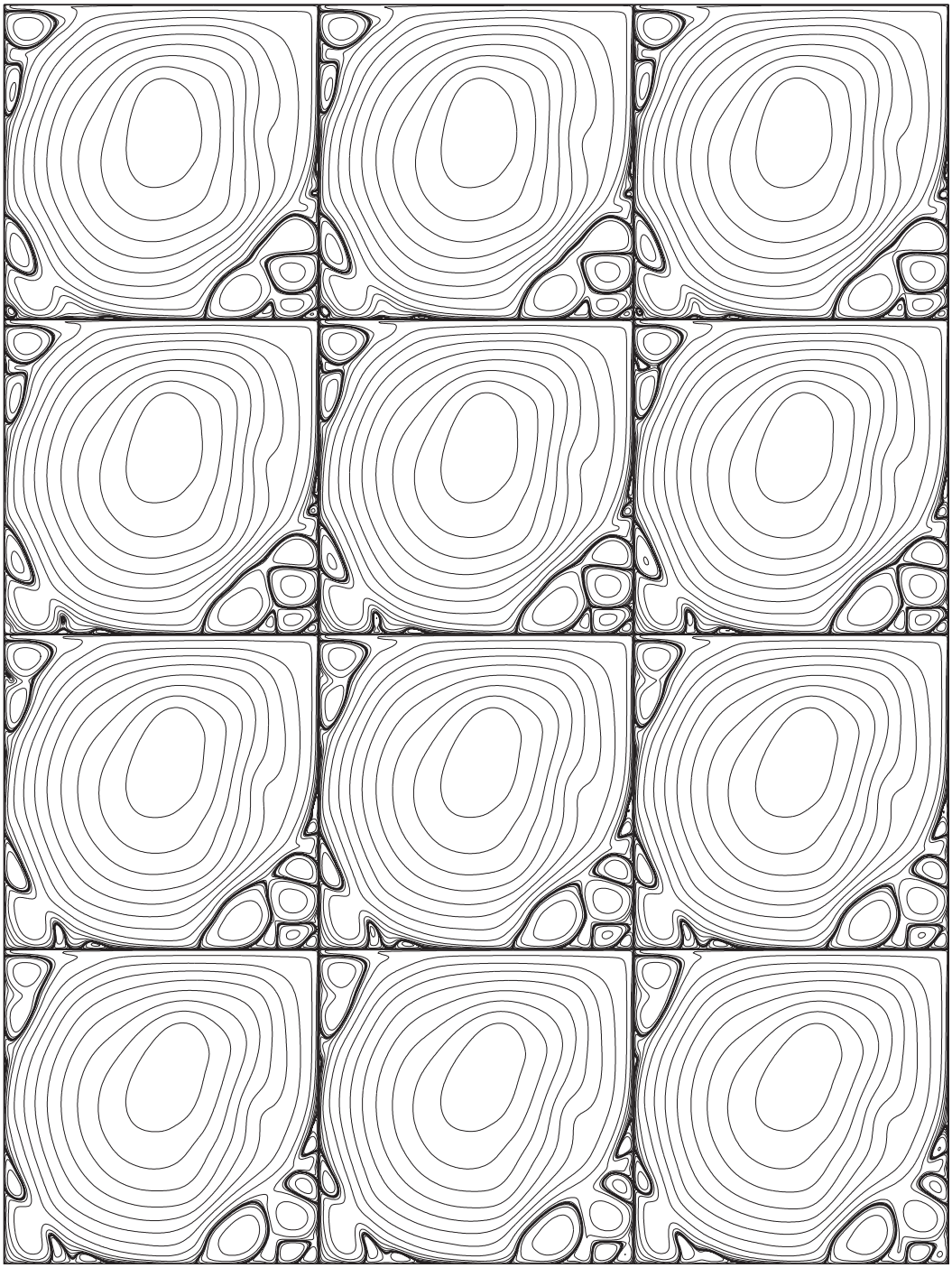

Figure 14: Re=30,000. h=1/256. Δt=3h. Chaotic solution. A particular occurrence.

drop upwards, the drop progresively vanishing. And then, the strong secondary vortex BL_2 begins absorbing the drop, the drop progresively strenghthening. Finally, the secondary vortex BL_2 absorbs the drop completely.

The case **Re**$=$**25, 000**. The solution becomes chaotic.

Fig. 13 displays a particular occurrence. The distinctive feature is a drop. At the top left corner. Two secondary vortices $\mathsf{left\_upTL}_2$ and $\mathsf{right\_upTL}_2$ form within the secondary vortex upTL_2. The sole interaction of the primary vortex with itself splits the secondary vortices $\mathsf{left\_upTL}_2$ and $\mathsf{right\_upTL}_2$, producing a drop, the secondary vortex $\mathsf{right\_upTL}_2$, which is dragged horizontally rightwards, progresively vanishing. This drop vanishes completely before reaching the horizontal center of the square cavity. The secondary vortex $\mathsf{left\_upTL}_2$ stands as the secondary vortex upTL_2.

Next, the long-term integration is performed with h=1/256, Δt=3h.

The case **Re**$=$**30, 000**. The solution becomes chaotic.

Fig. 14 displays a particular occurrence. The distinctive feature is the abrupt appearance of a secondary vortex. At the bottom left corner. The secondary vortex downBL_2 arises and begins growing, and right to the left, another secondary vortex $\mathsf{left\_downBL}_2$ arises and begins growing faster. And then, abruptly, just above the secondary vortex $\mathsf{left\_downBL}_2$ arises another secondary vortex $\mathsf{above\_left\_downBL}_2$. The secondary vortex $\mathsf{left\_downBL}_2$ catches and absorbs the secondary vortex $\mathsf{above\_left\_downBL}_2$, becoming the new secondary vortex $\mathsf{left\_downBL}_2$. Afterwards, the secondary vortices downBL_2 and $\mathsf{left\_downBR}_2$ merge, becoming the new secondary vortex downBL_2.

2.6 The time-step coarsening and the spatial-mesh-size refining

To make sure the time asymtotic regime of the flow has been reached, the long-term integration should attain a long time, so the use of a coarse time step should be helpful—but this introduces inherent numerical errors. Let us see how these modify the computed solution.

2.6.1 The effect of the time-step coarsening

The long-term integration is performed with h=1/256, Δt=4h which is compared with h=1/256, Δt=h.

The case **Re**$=$**7, 307.75**. The solution is time periodic, not stationary.

Fig. 15 displays this time periodic solution. The solution's behavior resembles for the most part the one at Re=7, 318 with h=1/256, Δt=h. Notwithstanding, the solution at Re=7, 307.75 with h=1/256, Δt=h is stationary, not time periodic. In fact, this is the last stationary solution just before the solutions turn out time periodic.

It appears that the inherent numerical errors due to the time-step coarsening add to the Reynolds number: The solution computed with a coarse time step Δt=4h at a Reynolds number corresponds to the solution computed with a fine time step Δt=h at a greater Reynolds number, the spatial mesh size fixed.

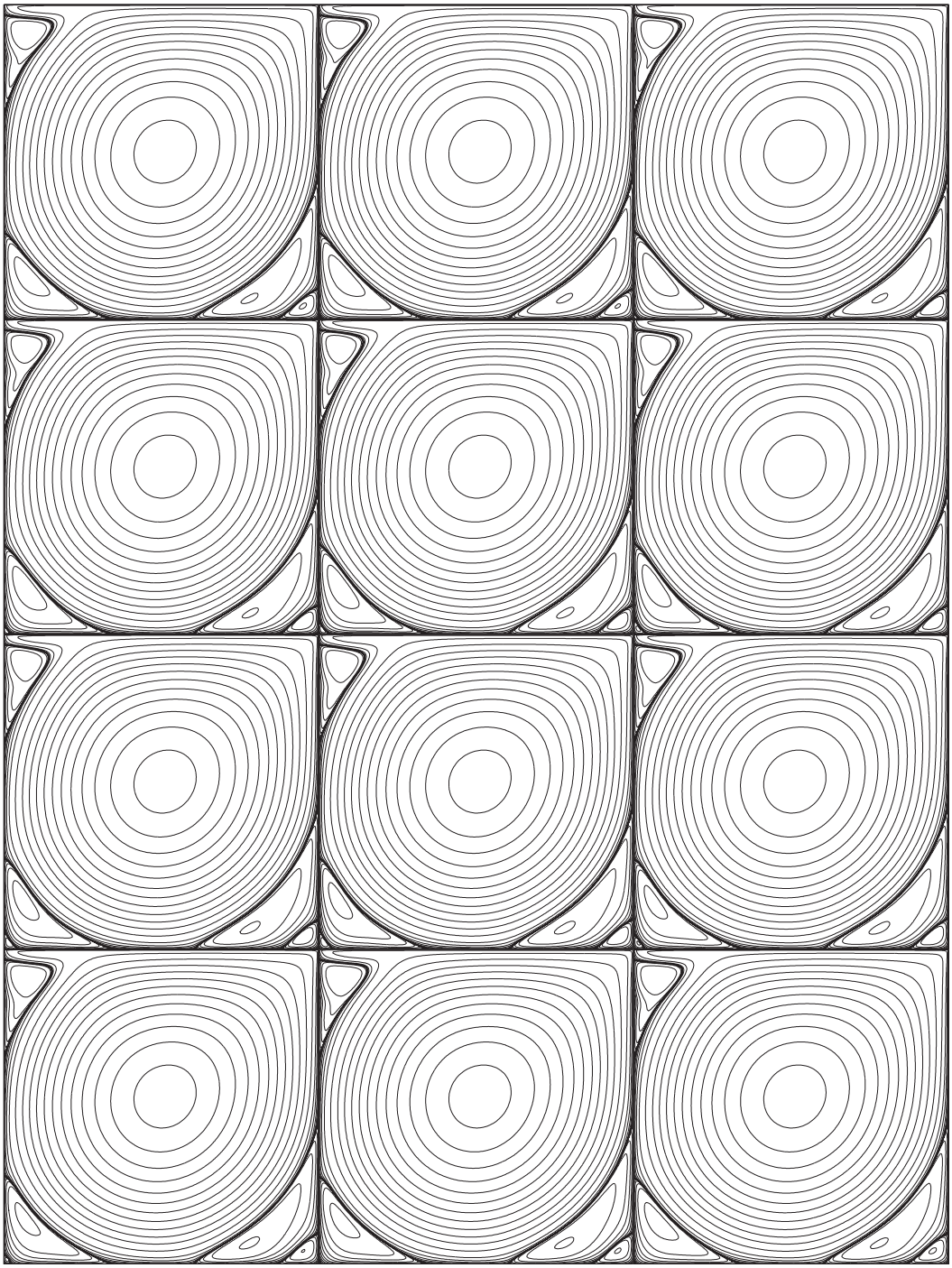

Figure 15: Re=7,307.75. h=1/256. Δt=4h. Time periodic solution.

On the other hand, the use of a finer spatial mesh size should produce more accurate solutions, but then their computation would be by far more expensive in CPU time, a severe drawback if the issue is the long-term integration. Yet, how relate the less precise computations performed with the coarse spatial mesh size $h=1/256$ to the more precise ones performed with the fine spatial mesh size $h=1/512$, the time step $\Delta t=4h$, for instance?

2.6.2 The effect of the spatial-mesh-size refining

The long-term integration is performed with $h=1/512$, $\Delta t=4h$ which is compared with $h=1/256$, $\Delta t=4h$.

The case **Re=12, 500**. The solution is time periodic.

Fig. 16 displays this time periodic solution. The solution's behavior resembles the one at Re=11,000 with $h=1/256$, $\Delta t=4h$.

But some pronounced differences arise.

At the bottom right corner. Two secondary vortices downBR_2 and upBR_2 keep merging and splitting as time goes on. The merging and splitting are not sharp. The secondary vortex upBR_2 and the quaternary vortex BR_4 arise almost simultaneously when the two secondary vortices downBR_2 and upBR_2 are about to split. Immediateley after the splitting, the tertiary vortex BR_3 becomes weak, and the primary vortex drags the secondary vortex upBR_2 downwards, to merge with the secondary vortex downBR_2—and the merging is not delayed. Meanwhile, the tertiary vortex downBR_3 and the quaternary vortex upBR_4 form out. Afterwards, when the two secondary vortices downBR_2 and upBR_2 are about to merge, the quaternary vortex BR_4 spreads vertically upwards along the right wall, not merging with the secondary vortex upBR_2, and horizontally leftward along the bottom wall, not merging with the secondary vortex downBR_2, and consequently not detaching the tertiary vortex BR_3 neither from the right wall nor from the bottom wall. Firstly, the secondary vortices upBR_2 and downBR_2 merge, becoming the secondary vortex BR_2. At this time, the quaternary vortex downBR_4 and the tertiary vortex upBR_3 form out. The quaternary vortices downBR_4 and upBR_4 do not split; the quaternary vortex downBR_4 becomes sharp. Secondly, the interaction of the secondary vortex BR_2 and the quaternary vortex downBR_4 splits the tertiary vortex BR_3, giving rise to the tertiary vortices downBR_3 and upBR_3. Simultaneously, the secondary vortex BR_2 and the quaternary vortex downBR_4 merge. Destroying the tertiary vortex downBR_3 and dragged further downwards by the primary vortex, the secondary vortex BR_2 becomes the secondary vortex BR_2 with the secondary vortex downBR_2 within. The tertiary vortex upBR_3 detached from the bottom wall but always clinging to the right wall becomes the tertiary vortex BR_3, the secondary vortex BR_2 dragging it upwards and making it to remain clung to the right wall. Just before the splitting of the tertiary vortex BR_3, the quinary vortex BR_5 arises. And then, the quaternary vortex upBR_4 drags the tertiary vortex BR_3 downwards, making it to cling to the bottom wall. The tertiary vortex BR_3 splits the secondary vortex BR_2 and the quaternary vortex upBR_4, giving rise to the quaternary vortex BR_4. Simultaneously,

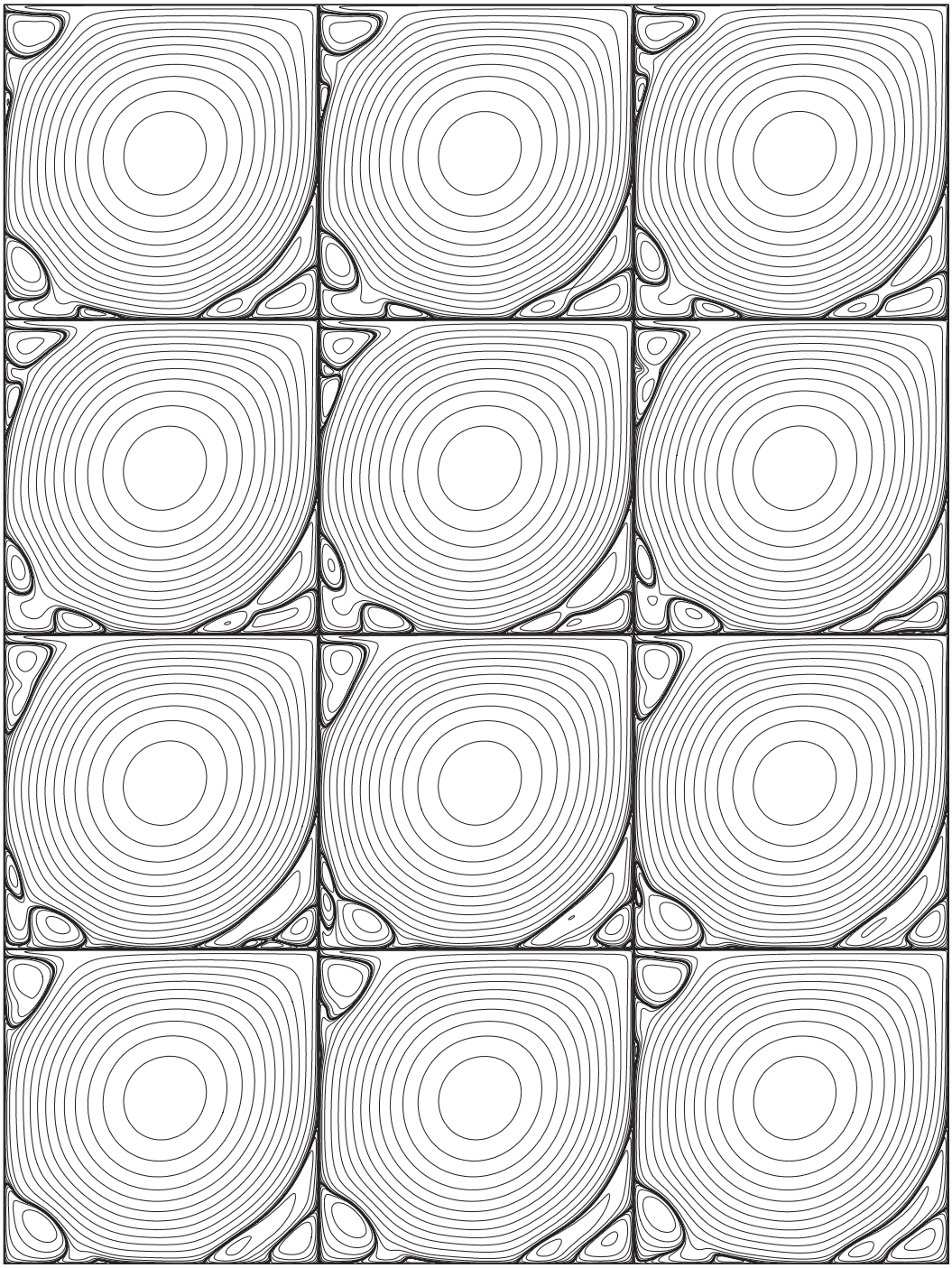

Figure 16: Re=12,500. h=1/512. Δt=4h. Time periodic solution.

the tertiary vortex BR_3 and the quinary vortex BR_5 merge, detaching the quaternary vortex BR_4 from the right wall. The quaternary vortex BR_4 remaining attached to the bottom wall vanishes promptly . The secondary vortex BR_2 with the secondary vortex downBR_2 within and the tertiary vortex BR_3 stand. And then, almost simultaneously, the secondary vortex upBR_2 and the quaternary vortex BR_4 arise. The tertiary vortex BR_3 becomes strong, and the interaction of the primary vortex and the tertiary vortex BR_3 splits the secondary vortices downBR_2 and upBR_2. This behavior repeats periodically. This is the secondary-secondary-quaternary vortex merging and splitting at the bottom right corner.

But what are those pronounced differences? Here, the primary vortex is flat—and the tertiary vortex upBR_3 do not detach from the right wall.

To summarize, the solution's behavior at a Reynolds number with $h=1/512$, $\Delta t=4h$ seems to resemble the one at a lesser Reynolds number with $h=1/256, \Delta t=4h$, but with some pronounced differences in the primary vortex and in the not detaching of the tertiary vortex upBR_3 from the right wall. In other words, a numerical experiment at a Reynolds number with $h=1/256, \Delta t=4h$ seems to predict the one at a greater Reynolds number with $h=1/512, \Delta t=4h$, making the former helpful for studying the time asymptotic regime of the flow.

3 Conclusions

For the three concerns of this research, the conclusions are:

• From Re=5,000 to Re=7,307.75 the solution is stationary. But at Re=7,308 the solution is time periodic, not stationary. So the critical Reynolds number for the first Hopf bifurcation localizes between Re=7,307.75 and Re=7,308. Time periodical behavior begins smoothly, imperceptibly at the bottom left corner: at a tiny tertiary vortex—all other vortices stay still, and then it spreads to the three relevant corners of the square cavity—all small vortices at all levels move periodically. The primary vortex stays still. On the same hand, at Re=13,393.5 the solution is time periodic; the long-term integration carried out past t_∞=126,562.5, the fluctuations of the kinetic energy look periodic—except slight defects. But at Re=13,393.75 the solution is not time periodic anymore: losing unambiguously, abruptly time periodicity, it becomes chaotic. So the critical Reynolds number for the second Hopf bifurcation localizes between Re=13,393.5 and Re=13,393.75.

• At high Reynolds numbers Re=20,000 until Re=30,000 the solution becomes chaotic, indeed. The long-term integration is carried out past the long time t_∞= 150,000, expecting the time asymptotic regime of the flow has been reached. The distinctive feature of the flow is then the appearance of drops: tiny portions of fluid produced by splitting of a secondary vortex, becaming loose and then fading away or being absorbed by another secondary vortex, promptly. At Re=30,000 another phenomenon arises—the abrupt appearance at the bottom left corner of a tiny secondary vortex, not produced by splitting of a secondary vortex.

• The numerical experiments above are performed with the spatial mesh size $h=1/256$ and with the time step $\Delta t=h$ to determine the first Hopf bifurcation or with the time step $\Delta t=4h$ to determine the second Hopf bifurcation. It appears that the inherent numerical errors due to the time-step coarsening add to the Reynolds number. On the other hand, A numerical experiment at a Reynolds number with $h=1/256$, $\Delta t=4h$ seems to predict the one at a greater Reynolds number with $h=1/512$, $\Delta t=4h$, making the former helpful for studying the time asymptotic regime of the flow. Spatial mesh size refining would produce mesh convergence of numerical solutions for h equal to or smaller than $h=1/2048$, however.

We close this paper by pointing out that the lid-driven square cavity flow—an almost fictitious flow [34]—has been solved many times by various techniques [2,3,13, 21,23,25,27,28,33,44], their results sometimes agreeing—at other times disagreeing [21, p. 927].

Acknowledgments

The author thanks Professor Roger Temam for providing the supercomputing support which allowed this research to be accomplished. This research was supported in part by the National Science Foundation Grant No. DMS-0604235.

References

[1] F. Auteri, N. Parolini and L. Quartapelle, *Numerical investigation on the stability of singular driven cavity flow*, J. Comput. Phys., 183(1) (2002), pp. 1–25.
[2] E. Barragy and G. F. Carey, *Stream function-vorticity driven cavity solution using p finite elements*, Comput. & Fluids, 26(5) (1997), pp. 453–468.
[3] C.-H. Bruneau and C. Jouron, *An efficient scheme for solving steady incompressible Navier-Stokes equations*, J. Comput. Phys., 89(2) (1990), pp. 389–413.
[4] C.-H. Bruneau and M. Saad, *The 2D lid-driven cavity problem revisited*, Comput. & Fluids, 35(3) (2006), pp. 326–348.
[5] M. Chen, A. Miranville and R. Temam, *Incremental unknowns in finite differences in three space dimensions* Comput. Appl. Math., 14(3) (1995), pp. 219–252.
[6] M. Chen and R. Temam, *The incremental unknown method I* , Appl. Math. Lett., 4(3) (1991), pp. 73–76.
[7] M. Chen and R. Temam, *The incremental unknown method II*, Appl. Math. Lett., 4(3) (1991), pp. 77–80.
[8] M. Chen and R. Temam, *Incremental unknowns for solving partial differential equations*, Numer. Math., 59(3) (1991), pp. 255–271.
[9] M. Chen and R. Temam, *Incremental unknowns for convection-diffusion equations*, Appl. Numer. Math., 11(5) (1993), pp. 365–383.
[10] M. Chen and R. Temam, *Incremental unknowns in finite differences: Condition number of the matrix*, SIAM J. Matrix Anal. Appl., 14(2) (1993), pp. 432–455.
[11] M. Chen and R. Temam, *Nonlinear Galerkin method in the finite difference case and wavelet-like incremental unknowns*, Numer. Math., 64(3) (1993), pp. 271–294.

[12] P. CONCUS, G. H. GOLUB, AND D. P. O'LEARY, *A generalized conjugate gradient method for the numerical solution of elliptic partial differential equations*, Sparse Matrix Computations, Academic Press, 1976. J. R. Bunch and D. J. Rose (Eds.).
[13] E. ERTURK, T. C. CORKE, AND C. GÖKÇÖL, *Numerical solutions of 2-D steady incompressible driven cavity flow at high Reynolds numbers*, Internat. J. Numer. Methods Fluids, 48(7) (2005), pp. 747–774.
[14] A. FORTIN, M. JARDAK, J. J. GERVAIS, AND R. PIERRE, *Localization of Hopf bifurcations in fluid flow problems*, Internat. J. Numer. Methods Fluids, 24(11) (1997), pp. 1185–1210.
[15] S. GARCIA, *The matricial framework for the incremental unknowns method*, Numer. Funct. Anal. Optim., 14(1&2) (1993), pp. 25–44.
[16] S. GARCIA, *Numerical study of the incremental unknowns method*, Numer. Methods Partial Differential Equations, 10(1) (1994), pp. 103–127.
[17] S. GARCIA, *Higher-order incremental unknowns, hierarchical basis, and nonlinear dissipative evolutionary equations*, Appl. Numer. Math., 19(4) (1996), pp. 467–494.
[18] S. GARCIA, *Algebraic conditioning analysis of the incremental unknowns preconditioner*, Appl. Math. Modelling, 22(4–5) (1998), pp. 351–366.
[19] S. GARCIA, *Incremental unknowns for solving the incompressible Navier-Stokes equations*, Math. Comput. Simulation, 52(5–6) (2000), pp. 445–489.
[20] S. GARCIA, *Incremental unknowns and graph techniques in three space dimensions*, Appl. Numer. Math., 44(3) (2003), pp. 329–365.
[21] S. GARCIA, *The lid-driven square cavity flow: From stationary to time periodic and chaotic*, Commun. Comput. Phys., 2(5) (2007), pp. 900–932.
[22] S. GARCIA AND F. TONE, *Incremental unknowns and graph techniques with in-depth refinement*, Int. J. Numer. Anal. Model., 4(2) (2007), pp. 143–177.
[23] U. GHIA, K. N. GHIA AND C. T. SHIN, *High-Re solutions for incompressible flow using the Navier-Stokes equations and a multigrid method*, J. Comput. Phys., 48(3) (1982), pp. 387–411.
[24] R. GLOWINSKI, *Finite Element Methods for the Numerical Simulation of Incompressible Viscous Flow. Introduction to the Control of the Navier-Stokes Equations*, vol. 28 of Lectures in Applied Mathematics, American Mathematical Society, 1991.
[25] O. GOYON, *High-Reynolds number solutions of Navier-Stokes equations using incremental unknowns*, Comput. Methods Appl. Mech. Engrg., 130(3–4) (1996), pp. 319–335.
[26] F. H. HARLOW AND J. E. WELCH, *Numerical calculation of time-dependent viscous incompressible flow of fluid with free surface*, Phys. Fluids, 8(12) (1965), pp. 2182–2189.
[27] J. KIM AND P. MOIN, *Application of a fractional-step method to incompressible Navier-Stokes equations*, J. Comput. Phys., 59(2) (1985), pp. 308–323.
[28] M. LI, T. TANG, AND B. FORNBERG, *A compact fourth-order finite difference scheme for the steady incompressible Navier-Stokes equations*, Internat. J. Numer. Methods Fluids, 20(10) (1995), pp. 1137–1151.
[29] Y.-F. PENG, Y.-H. SHIAU, AND R. R. HWANG, *Transition in a 2-D lid-driven cavity flow*, Comput. & Fluids, 32(3) (2003), pp. 337–352.
[30] P. POULLET, *Staggered incremental unknowns for solving Stokes and generalized Stokes problems*, Appl. Numer. Math., 35(1) (2000), pp. 23–41.
[31] M. SAHIN AND R. G. OWENS, *A novel fully-implicit finite volume method applied to the lid-driven cavity problem, Part II. linear stability analysis*, Internat. J. Numer. Methods Fluids, 42(1) (2003), pp. 79–88.
[32] V. SARIN AND A. SAMEH, *An efficient iterative method for the generalized Stokes problem*, SIAM J. Sci. Comput., 19(1) (1998), pp. 206–226.
[33] R. SCHREIBER AND H. B. KELLER, *Driven cavity flows by efficient numerical techniques*, J.

Comput. Phys., 49(2) (1983), pp. 310–333.
[34] P. N. SHANKAR AND M. D. DESHPANDE, *Fluid mechanics in the driven cavity*, Annu. Rev. Fluid Mech., 32 (2000), pp. 93–136.
[35] A. SMITH AND D. SILVESTER, *Implicit algorithms and their linearisation for the transient incompressible Navier-Stokes equations*, IMA J. Numer. Anal., 17(4) (1997), pp. 527–545.
[36] L. SONG AND Y. WU, *Incremental unknowns in three-dimensional stationary problem*, Numer. Algorithms, 46(2) (2007), pp. 153–171.
[37] L. SONG AND Y. WU, *Incremental unknowns method based on the θ-scheme for time-dependent convection-diffusion equations*, Math. Comput. Simulation, 79(7) (2009), pp. 2001–2012.
[38] P. N. SWARZTRAUBER, *The methods of cyclic reduction, Fourier analysis and the FACR algorithm for the discrete solution of Poisson's equation on a rectangle*, SIAM Rev., 19(3) (1977), pp. 490–501.
[39] R. A. SWEET, *Direct methods for the solution of Poisson's equation on a staggered grid*, J. Comput. Phys., 12(3) (1973), pp. 422–428.
[40] R. TEMAM, *Inertial manifolds and multigrid methods*, SIAM J. Math. Anal., 21(1) (1990), pp. 154–178.
[41] R. TEMAM, Infinite Dimensional Dynamical Systems in Mechanics and Physics, Applied Mathematical Sciences. Springer-Verlag, 1997.
[42] R. TEMAM, Navier-Stokes Equations: Theory and Numerical Analysis, AMS Chelsea Publishing. American Mathematical Society, 2001.
[43] H. A. VAN DER VORST, *Bi-CGSTAB: a fast and smoothly converging variant of Bi-CG for the solution of nonsymmetric linear systems*, SIAM J. Sci. Statist. Comput., 13(2) (1992), pp. 631–644.
[44] S. P. VANKA, *Block-implicit multigrid solution of Navier-Stokes equations in primitive variables*, J. Comput. Phys., 65(1) (1986), pp. 138–158.
[45] Y.-J. WU AND A.-L. YANG, *Incremental unknowns for the heat equation with time-dependent coefficients: semi-implicit θ-schemes and their stability*, J. Comput. Math., 25(5) (2007), pp. 573–582.